Virus Research 157 (2011) 35–46

Contents lists available at ScienceDirect

Virus Research

journal homepage: www.elsevier.com/locate/virusres

Engineered *Tobacco mosaic virus* mutants with distinct physical characteristics *in planta* and enhanced metallization properties

Anan Kadri[a,*], Edgar Maiß[b], Nadja Amsharov[c], Alexander M. Bittner[c,1], Sinan Balci[c], Klaus Kern[c], Holger Jeske[a], Christina Wege[a,**]

[a] Universität Stuttgart, Institute of Biology, Department of Plant Molecular Biology and Plant Virology, Pfaffenwaldring 57, D-70550 Stuttgart, Germany
[b] Leibniz Universität Hannover, Institut für Pflanzenkrankheiten und Pflanzenschutz, Herrenhäuser Straße 2, D-30419 Hannover, Germany
[c] Max Planck Institute for Solid State Research, Heisenbergstraße 1, D-70569 Stuttgart, Germany

ARTICLE INFO

Article history:
Received 22 July 2010
Received in revised form 25 January 2011
Accepted 29 January 2011
Available online 15 February 2011

The publication is dedicated to Karl-Wolfgang Mundry, founder of the Plant Virology Department at the University of Stuttgart, who deceased in 2009.

Keywords:
Tobacco mosaic virus (TMV)
Coat protein
Mutation
Nanotechnology
Metallization

ABSTRACT

Tobacco mosaic virus mutants were engineered to alter either the stability or surface chemistry of the virion: within the coat protein, glutamic acid was exchanged for glutamine in a buried portion to enhance the inter-subunit binding stability (E50Q), or a hexahistidine tract was fused to the surface-exposed carboxy terminus of the coat protein (6xHis). Both mutant viruses were expected to possess specific metal ion affinities. They accumulated to high titers in plants, induced distinct phenotypes, and their physical properties during purification differed from each other and from wild type (wt) virus. Whereas 6xHis and wt virions contained RNA, the majority of E50Q protein assembled essentially without RNA into rods which frequently exceeded 2 μm in length. Electroless deposition of nickel metallized the outer surface of 6xHis virions, but the central channel of E50Q rods, with significantly more nanowires of increased length in comparison to those formed in wtTMV.

1. Introduction

Tobacco mosaic virus (TMV) is the type member of the genus *Tobamovirus*. Its virion encapsidates a helical plus-sense single-stranded RNA (+ssRNA) genome of 6395 nucleotides in 2130 identical coat protein subunits of 17.5 kDa each, and forms a rigid helical tube with a length of 300 nm, a diameter of 18 nm, and a central channel 4 nm in width. As this structure exposes several distinct and repeated functional groups on the inner and outer surfaces (Clare and Orlova, 2010; Klug, 1999; Namba et al., 1989; Sachse et al., 2007) it is suitable for differential modifications such as metallization and has therefore been the subject of intensive studies in the field of nanotechnology as a versatile biotemplate, yielding an ever increasing number of close-to-application materials and devices (e.g. Balci et al., 2007, 2008, 2009; Dujardin et al., 2003; Gerasopoulos et al., 2010; Górzny et al., 2010; Knez et al., 2002, 2003, 2004a,b, 2006; Kobayashi et al., 2010; Lee et al., 2006; Lim et al., 2010; Miller et al., 2007; Rong et al., 2009; Royston et al., 2008, 2009; Schlick et al., 2005; Shenton et al., 1999; Smith et al., 2006; Tseng et al., 2006; Wu et al., 2010a; Yang et al., 2010; Yi et al., 2005).

TMV exists in a great number of different strains and mutants and accumulates to high levels in many host plants with variable symptom responses (reviewed in Culver, 2002; Zaitlin and Israel, 1975). Dependent on both the virus strain and the host genome, it may either spread systemically, or may be restricted to a local infection site, and induce yellowing, mosaic, severe systemic necrosis, or local necrotic lesions (Mundry et al., 1990; Zaitlin and Israel, 1975). Wild type (wt) virions are exceptionally stable under a broad range of chemical and physical conditions (Mutombo et al., 1992; Perham and Wilson, 1978; Zaitlin, 2000) and easily isolated from plants, but changes in the coat protein sequence may disrupt particle stability and impede purification.

* Corresponding author. Tel.: +49 711 685 65072; fax: +49 711 685 65096.
** Corresponding author. Tel.: +49 711 685 65073; fax: +49 711 685 65096.
E-mail addresses: anan.kadri@bio.uni-stuttgart.de (A. Kadri), christina.wege@bio.uni-stuttgart.de (C. Wege).
[1] Present address: CIC nanoGUNE Consolider, Tolosa Hiribidea 76, E-20018 Donostia - San Sebastian, and IKERBASQUE, Basque Foundation for Science, E-48011 Bilbao, Spain.

0168-1702/$ – see front matter © 2011 Elsevier B.V. All rights reserved.
doi:10.1016/j.virusres.2011.01.014

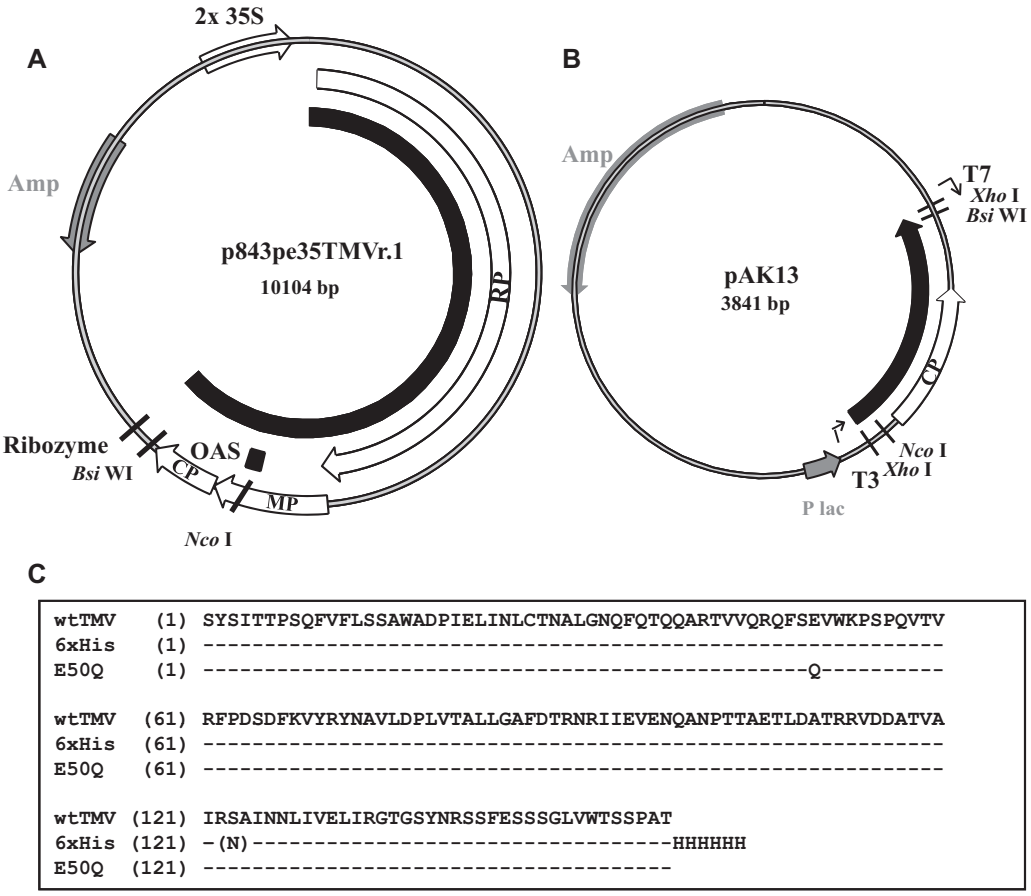

Fig. 1. Constructs and sequences used. Genetic maps at different scales for the infectious wtTMV plasmid construct p843pe35TMVr.1 (A) or the mutagenesis sub-clone pAK13 (B), and alignment of the TMV CP amino acid sequences (C). Genetic elements and restriction sites used in cloning strategies, mutagenesis and to generate TMV CP-specific probes are indicated: RP, RNA-dependent RNA polymerase; MP, movement protein; CP, coat protein; OAS, origin of assembly. The resulting transcripts for the full-length TMV genome and the TMV fragment (nts 5433-6306; NC 001367) are indicated by black arcs. Alignment of the CP amino acid sequences (C) deduced from the nucleotide sequences of the indicated constructs.

The virion structure (Clare and Orlova, 2010; Namba et al., 1989; Sachse et al., 2007) provides some explanation for its stability. Carboxyl–carboxylate interactions tighten adjacent coat protein subunits, and carboxylate–phosphate pairs bind protein subunits to RNA (reviewed in Culver, 2002). Upon infection, virions face physiological conditions with lower calcium concentrations and higher pH values than in the extracellular environment, and protons as well as calcium ions are removed from the carboxyl–carboxylate and carboxylate–phosphate pairs. The resulting repulsive negative electrostatic charges destabilize the subunits' interactions (Caspar, 1963; Caspar and Namba, 1990), and permit disassembly necessary for translation and replication. Hence, one of the so-called "Caspar-carboxylate" groups (glutamic acid at position 50) was changed to glutamine in this study, in order to stabilize the rod structure and prevent its disassembly as described (Bendahmane et al., 2007; Culver et al., 1995; Lu et al., 1996), to improve the robustness of the biotemplate for metallization purposes.

In addition, amino acids may be replaced or inserted at the C-termini, the N-termini, or within the exposed loop in order to functionalize the outer surface of the virion specifically (Lee et al., 2005, 2006; Smith et al., 2006; Yi et al., 2005). Thus, in order to exploit the well-known binding affinity of histidine to nickel, cobalt or zinc, a hexahistidine oligopeptide was fused to the C-terminus of the coat protein. The stabilities and metal-binding properties of both mutants compared to those of wtTMV virions are discussed.

2. Materials and methods

2.1. Construction of infectious clones for TMV coat protein mutants

cDNA was generated from the RNA of wt full-length TMV vulgare strain (PV0107; DSMZ, Germany), inserted into the bacterial plasmid pT7T3 19U (Pharmacia) between a duplicated *Cauliflower mosaic virus* 35S promoter (Restrepo et al., 1990) and a hammerhead ribozyme (Shintaku et al., 1996) using standard cloning procedures (Sambrook and Russell, 2001), resulting in the plant-infectious plasmid p843pe35TMVr.1 (Fig. 1A).

To generate mutants, a sub-clone (pAK13, Fig. 1B) comprising nucleotides 5433 to 6306 of TMV cDNA was raised from p843pe35TMVr.1 using pBluescript-SKII + (Stratagene, Heidelberg, Germany) as vector: the corresponding 874 bp cDNA fragment was amplified by PCR [95 °C, 5 min; 25 cycles 95 °C, 30 s, 72 °C, 30 s, 72 °C, 1 min; 72 °C, 10 min] using Taq DNA polymerase (Qiagen, Hilden, Germany), forward primer #1 and reverse primer #2, each adding an *Xho* I restriction site (Table 1), and inserted into the same restriction site of the vector following standard protocols (Sambrook and Russell, 2001). Mutants were raised by PCR amplification of the entire sub-clone pAK13 in the presence of mutant primers and blunt-end re-ligation, for pAK-6xHis using Taq DNA polymerase (Qiagen) with primers #3 and #4 [95 °C, 5 min; 25 cycles 95 °C, 30 s, 72 °C, 30 s, 72 °C, 3 min; 72 °C, 7 min], or for pAK-E50Q using proofreading DNA polymerase (Qiagen) and primers #5

Table 1
PCR primers used for TMV CP cloning, mutagenesis, sequencing, or RT-PCR.

#	Name	Sequence[a] (5′ to 3′)
1	5′AKp843TMVXhoI5433a	CCAACCTCGAGGATTACAAACGTGAGAGACGGAGG
2	3′AKp843TMVXhoI6306b	CCAACCTCGAGCGCGATCCAAGACACAACCCTTCG
3	5′AKpBlCPTMV6206Ma	ATAATAAATAACGGATTGTGTCCGTAATCACACGTGGTGCGTACGATAACGC
4	3′AKpBlCPTMV6205Mb	GCATCTTGACTAGCTCA(**ATGGTG**)$_3$AGTTGCAGGACTAGAGG
5	5′AKpBlCPTMV5851Ma	GACAATTCAGTCAGGTGTGGAAACC
6	3′AKpBlCPTMV5850Mb	TTTGAACGACAGTTCGAGCTTGTTG
7	AKcpTMVseq5680.MF	GCTACTTGTCGCCGAATCGGATTCG
8	AKcpTMVseq5971.MR	GCACCTAACAGTGCTGTGACTAGC
9	AKcpTMVseq5362.F	CCGCTTTCTCTGGAGTTTGTGTCG
10	AKcpTMVseq6346.R	CGTGCCTGCGGATGTATATGAACC′

[a] Added restriction sites are underlined. Inserted or altered sequences are bold.

and #6 [95 °C, 5 min; 25 cycles 94 °C, 45 s, 68 °C, 30 s, 72 °C, 4 min; 72 °C, 10 min]. Correctness of the resultant clones was confirmed by sequencing using a semi-automatic system (LI-COR Biosciences GmbH, Bad Homburg, Germany) and IRD-labeled primers (Table 1) #7 or #8 after cycle-sequencing reactions [92 °C, 2 min; 30 cycles 92 °C, 15 s, 64 °C for primer #7 or 54 °C for primer #8, 15 s, 70 °C, 30 s]. Accurate sub-clones were digested with *Nco* I and *Bsi* WI and the smaller fragment was inserted into the *Nco* I/*Bsi* WI fragment of the infectious plasmid p843pe35TMVr.1 yielding the infectious mutant clones pTMVcp6xHis and pTMVcpE50Q. Their sequences were verified using primers #7 and #8 (as above), and #9 or #10 (annealing temperature of 61 °C). The resultant final TMV mutants 6xHis and E50Q were used in all subsequent analyses.

2.2. Virus propagation and infectivity assays

Seeds of test plants were germinated in soil and maintained under greenhouse conditions with auxiliary lighting (24 °C/16 h day period and 18 °C/8 h night period). TMV CP mutants (6xHis or E50Q) and wtTMV were propagated in *Nicotiana tabacum* L. cv. 'Samsun' nn or NN, 'Xanthi' nc, *Nicotiana benthamiana* Domin, *Nicotiana rustica* L. and *N. rustica*. L. cv. 'Pavonii' and 'Cordata'. Two upper leaves (No. 4 and 5) of plants in the five to six leaf-stage were mechanically inoculated using Carborundum® as an abrasive with infectious plasmid DNA (1 μg per leaf diluted in 100 mM sodium potassium phosphate buffer [SPP], pH 7.4, prepared according to Sambrook and Russell, 2001). For lesion assays on 'Samsun' NN and 'Xanthi' nc, 1 or 0.5 μg of the corresponding infectious cDNAs was applied per half of same leaves; additionally, plant sap from symptomatic *N. benthamiana* upper leaves (prepared from 10 mg infected material in 100 μl SPP per inoculated leaf) was used on separate plants. Inoculated or buffer-treated control plants were maintained in a greenhouse under 20 °C/16 h light and 15 °C/8 h dark periods.

2.3. Virus enrichment and purification

Two methods for virus isolation were compared.

Method A. Slightly modifying the protocol of Devash et al. (1981), virus was purified from symptomatic plants (*N. tabacum* cv. 'Samsun' nn, 14, 21 and 28 dpi) by differential and density-gradient centrifugation. Young systemically infected leaves (20 g) were harvested and homogenized (blender) with three volumes per g fresh weight in 0.1 M EDTA pH 8.0 at 4 °C. The homogenate was filtered through two layers of gauze, and the filtrate centrifuged (5300 × *g*, 15 min, 4 °C, Sorvall, SLA-1500 rotor). The resultant supernatant was filtered through a 1 cm thick layer of Celite® (545, 0.02-0.1 mm grain size, Merck Biosciences, Bad Soden, Germany). The resulting filtrate was incubated for 90 min at 50 °C. Denatured plant proteins were removed by sedimentation (as above). The supernatant was centrifuged (117,000 × *g*, 90 min, 4 °C, Beckman, Ti 60 rotor) and the sediment resuspended in 10 mM SPP (pH 7.0) using 0.5 ml per g initial plant tissue. Virus particles were separated from aggregates by low-speed centrifugation (4800 × *g*, 10 min, 4 °C, Sorvall, SLA-1500 rotor). The supernatant was either loaded onto sucrose gradients for rate-zonal centrifugation or for isopycnic centrifugation.

Method B. Virus particles were isolated from *N. benthamiana* following the procedure of Chapman (1998). Frozen (−70 °C) systemically infected leaves (5 g) from symptomatic plants (21 and 28 dpi) were pulverized with mortar and pestle in 50 ml 100 mM SPP and filtered through three layers of gauze. Aliquots of each purification step were kept for further analysis and the remainder processed as follows: filtrates (F; 12.5 ml) were centrifuged (5000 × *g*, 15 min, 18 °C, Sorvall, SS34 rotor), from which pellets (P1) and supernatants (S1) were separated, *n*-butanol (final concentration [f.c.] of 8%) was added dropwise to the supernatants while stirring the mixture at room temperature (RT) for 45 min prior to its clarification by centrifugation (10,000 × *g*, 30 min, 4 °C, Sorvall, SS34 rotor). The resulting pellets were resuspended (P2), the upper butanol phases discarded, and the supernatants filtered through Miracloth® (S2).

2.3.1. Rate-zonal centrifugation in sucrose density gradients

Samples (0.5–1 ml) were layered onto 10–30% sucrose gradients, centrifuged (32,000 rpm, 2.5 h, 4 °C, Beckman, SW40 rotor) and fractionated into 33 aliquots into microtiter plates. Absorbance profiles (A_{260}, A_{280} and A_{320}) were recorded for the fractions and the resuspended pellets. Selected fractions were pooled (50 μl each), dialyzed against 10 mM SPP buffer at 4 °C, and analyzed by Western blotting and electron microscopy.

2.3.2. Isopycnic density-gradient centrifugation in the presence of Cs_2SO_4

Samples were diluted to a final volume of 13.5 ml 100 mM SPP and adjusted to 35% Cs_2SO_4 (w/v) and centrifuged (16,000 × *g*, 10 min, 20 °C, Sorvall, HB6 rotor) to remove aggregated material. The resulting supernatants were centrifuged to equilibrium density (50,000 rpm, 17 h, 20 °C, Beckman, VTi65.1 rotor) and 36 fractions of 400 μl were collected from the bottom of the tubes. Their absorbance profiles (A_{260}, A_{280} and A_{320}) were monitored using a SPECTRAFluor plus spectrophotometer (TECAN, Crailsheim, Germany) and their virus content by enzyme-linked immunosorbent assay (ELISA).

2.4. Nucleic acid isolation, RT-PCR and sequencing

Total nucleic acids were purified from young, systemically infected *N. tabacum* cv. 'Samsun' nn leaves, or inoculated tobacco 'Samsun' NN leaves exhibiting local lesions (100 mg each), at 14, 21 and 28 dpi according to Boom et al. (1990). TMV RNA from purified TMV particles was obtained by means of phenol/chloroform extraction and alcohol precipitation.

RNA samples were reverse-transcribed using an AMV first-strand cDNA synthesis kit (Invitrogen, Karlsruhe, Germany) and TMV primer #2 (Table 1) following the manufacturer's instructions. One tenth of the volume of cDNA (2 μl) and the primers #1 and #2 were used for PCR [95 °C, 5 min; 35 cycles of 95 °C, 45 s, 56 °C, 45 s, 72 °C, 1 min; 72° C, 10 min]. Fragments from 15 μl samples of the PCR reaction were separated in 0.8% agarose gels in TBE (89 mM Tris, 89 mM boric acid, 2 mM EDTA), eluted and sequenced.

2.5. TMV-specific probe

To obtain a TMV-plus-strand-specific probe, pAK13 was digested with *Hin*d III and transcribed *in vitro* using T7 polymerase (DIG-RNA labeling kit (SP6/T7), Roche Applied Science, Penzberg, Germany).

2.6. RNA extraction and Northern blot analysis

For total nucleic acids isolated from plant tissues, samples (15 μl) were separated on 1% agarose/MOPS gels and transferred to nylon membranes (Hybond-NX, Amersham Biosciences, NJ, USA) according to Sambrook and Russell (2001). RNA was hybridized with a DIG-labeled probe specific for TMV CP RNA, and signals were developed according to the DIG system user's guide for filter hybridization (Roche Applied Science).

For RNA extraction from TMV particles, samples (33 μl) from each step of the virus isolation (method B) were treated with a mixture of 1 μl proteinase K (10 mg/ml, Sigma–Aldrich, Munich, Germany) and 32 μl solution of 2% SDS, 0.3 M NaCl, 0.1 M EDTA, 2% bentonite for 20 h at45 °C and centrifuged (13,000 rpm, 5 min, Eppendorf, 5417C rotor). Supernatants (2 μl) were treated with 2.5% SDS (f.c.) for 10 min at 65 °C, separated on 1% agarose/0.03% SDS gels, transferred to nylon membranes, and the RNA was detected as above.

2.7. Polyacrylamide gel electrophoresis (PAGE) and Western blot analysis

Electrophoresis and Western blotting were performed according to standard methods (Laemmli, 1970; Towbin et al., 1979). Samples were denatured by boiling in Laemmli sample buffer (100 mM Tris–HCl pH 6.8, 4% SDS, 0.2% bromophenol blue, 20% glycerin, 200 mM DTT), electrophoresed using 15% polyacrylamide gels, stained with Serva-Violet 17 (SERVA Electrophoresis GmbH, Heidelberg, Germany) or electro-blotted to nitrocellulose membranes (Protran BA85, Schleicher & Schuell, Dassel, Germany). Blots were blocked with 5% (w/v) nonfat milk powder for at least 1 h at RT, incubated with TMV-specific rabbit IgG (kindly provided by Prof. K.W. Mundry, Stuttgart, Germany, diluted 1/1000) or anti-pentaHis mouse antibodies (Biotrend, Cologne, Germany). Goat anti-rabbit IgG or rabbit anti-mouse IgG conjugated with alkaline phosphatase (Biotrend, Cologne, Germany) were used as secondary antibodies. Enzyme activity was detected using NBT/BCIP (nitro blue tetrazolium chloride/5-bromo-4-chloro-3-indolyl phosphate, toluidine salt) or CDP-star® (Roche Applied Science).

2.8. Enzyme-linked immunosorbent assay (ELISA)

Aliquots (50 μl) of each fraction from the density gradients were analyzed by ELISA according to standard procedures using Greiner high-binding plates (Greiner Bio-One International AG, Frickenhausen, Germany) and rabbit anti-TMV IgG (1/1000 dilution) and alkaline phosphatase-conjugate (goat anti-rabbit IgG, Biotrend; 1/5000). Between treatments, plates were washed with phosphate-buffered saline supplemented with 0.05% Tween-20. After adding substrate (100 μl *p*-nitrophenyl phosphate, 1 mg/ml) to each well, enzyme activity was measured at A_{405} using a SPECTRAFluor Plus spectrophotometer (TECAN).

2.9. Electron microscopy

Samples were adsorbed on Formvar®/carbon-coated 400-mesh grids, rinsed with 40 drops of ddH_2O and negatively stained with 1% aqueous uranyl acetate containing 250 μg/ml bacitracin. Immunosorbent electron microscopy (ISEM) (Milne and Lesemann, 1984) was performed by coating grids with antibodies (rabbit anti-TMV IgG or mouse anti-pentaHis monoclonal IgG (Qiagen, Hilden)) diluted 1/1000 in 10 mM phosphate buffer, pH 7 for 15 min. The coated grids were incubated with samples for 15 min at RT, rinsed with water and negatively stained as described above.

2.10. Metallization of TMV particles with nickel

Electroless metal deposition was applied to the different virus variants following a slightly modified method on the basis of Balci et al. (2006). For activation with Pd(II), samples (50 μl) from filtrates (F, see above) of wt or mutant TMV-infected plant material, respectively, were diluted with H_2O (250 μl), dialyzed twice against H_2O (10 min, Slide-A-Lyzer 10,000 MWCO), incubated (10 min, RT) with an equal volume of freshly prepared activation bath (1.36 mM Na_2PdCl_4, 1 M NaCl) at pH 7.0 and centrifuged (13,000 rpm, 10 min, Eppendorf, 5417C rotor). The resulting brownish pellets were washed with H_2O, sedimented (13,000 rpm, 5 min, Eppendorf, 5417C rotor) and resuspended in 300 μl H_2O. For nickel electroless deposition, the Pd-activated suspensions were mixed with an equal volume of metallization solution (223 mM $Ni(CH_3COO)_2{\cdot}4H_2O$, 228 mM lactic acid, 42.4 mM $(CH_3)_2NH{\cdot}BH_3$, adjusted to pH 7.5 with NaOH). Aliquots were taken as soon as metal was observed, immediately adsorbed on Formvar®/carbon-coated 400-mesh grids, incubated for 2 min and analyzed by electron microscopy.

2.11. MALDI-MS analysis

Systemically infected leaves (200 mg) from symptomatic plants (21 dpi) were pulverized with mortar and pestle in 2 ml 100 mM SPP and filtered through three layers of gauze; samples from each filtrate (F), pellet (P1 and P2) and second supernatant (S2) were prepared for MALDI-MS analysis. Viruses were denatured by adding 6 μl guanidine hydrochloride (6 M) to the sample (24 μl) and mixing for 5 min at RT. Denatured proteins were spotted on MTP 384 massive target plate using Millipore $ZipTips_{C18}$® tips (Millipore Corporation Billerica, USA) to remove excess salts and assist the binding of protein to the sinapic acid matrix (Sigma–Aldrich, Germany). MALDI-TOF-MS analysis was performed using a Bruker reflex IV mass spectrometer (Bruker Daltonics, Germany) and linear positive mode.

3. Results

3.1. Infectious constructs

The TMV CP gene was amplified from the infectious full-length construct p843pe35TMVr.1 (Fig. 1A), and TMV CP mutants 6xHis (hexahistidine at the C-terminus) and E50Q (amino acid substitution at position 50) were generated in pAK13 (Fig. 1B), giving pAK-6xHis and pAK-E50Q. Their inserts were transferred back in place of the wt CP gene of the infectious construct, giving pTMVcp6xHis and pTMVcpE50Q. The first resulting clones carried an unintended second mutation (S123N) in pAKcp6xHis-1, which

Table 2
Numbers and diameters of local lesions on N gene-carrying tobacco induced by infectious plasmid DNA, or by plant sap from systemically infected *N. benthamiana* leaves for different TMV variants, analyzed at 7 or 2 days post inoculation, respectively.

Inoculum	Infectious cDNA				Plant sap			
Host	*Samsun NN*		*Xanthi nc*		*Samsun NN*		*Xanthi nc*	
TMV variant	LL	*D*	LL	*D*	LL	*D*	LL	*D*
wtTMV	2.7	0.5–2.0	4.4	1.0	850	1.0–1.5	800	1.0–1.5
TMV-E50Q	2.9	0.5–2.0	4.5	3.5	1.0	0.5	1.0	1.0
TMV-His_6	1.2	0.2–1.0	5.0	1.5–2.0	180	0.2–1.0	200	0.5–1.0
TMV-His_6 (+S123N)	0	–	0	–	0	–	0	–

Average numbers of local lesions, and ranges of their diameters on locally infected leaves of the indicated hosts. LL: local lesions per leaf (decimals omitted for values >10); *D*: diameter in mm.

was absent from a second construct (pAKcp6xHis-2) generated by use of a proofreading DNA-polymerase (Fig. 1C, and sequencing data not shown). Both variants of the 6xHis mutant behaved similarly in the subsequent analysis, except for a distinct response induced in local lesion hosts (see below), indicating that the S123N exchange did not have any detectable influence on properties of the mutants' systemic infection and physicochemical characteristics of the virions.

All constructs were inoculated onto plants for virus propagation. Initial infectivity assays were carried out with *Nicotiana tabacum* 'Samsun' nn or NN (referred to as nn, NN tobacco in the following). Following mechanical inoculation of plasmid DNA, E50Q induced typical systemic mosaic symptoms on nn tobacco like wtTMV (not shown), but delayed (at 21 dpi compared to 14 dpi for wtTMV). However, mosaic development stopped later on, and no symptoms were observed on newly developed leaves beyond 40 dpi. On the inoculated leaves of NN and nc tobacco, E50Q-infectious plasmid induced local lesions, the number and size of which did not significantly differ from those elicited by wtTMV plasmid (see Table 2). 6xHis revealed inconspicuous up to mild symptoms at 21 dpi on the systemic host. A lower number of lesions of slightly reduced diameter on plants with the N gene were generated by 6xHis (Table 2). The clone pAKcp6xHis-1 harboring the second-site CP mutation S123N, however, did not yield any lesions. A second set of local lesion assays was carried out using plant sap from systemically invaded *N. benthamiana* leaves as inoculum. These results (Table 2) confirmed that the accurate 6xHis mutant provoked less local lesions than wtTMV (in contrast to the 6xHis + S132N clone lacking lesions). Plant sap from E50Q-infected *N. benthamiana* produced only negligible numbers of local lesions in the same assay.

Total RNAs were isolated from leaves with local lesions from NN, and from systemic leaves from nn tobacco and analyzed by RT-PCR and sequencing. For E50Q, viral RNA was successfully obtained from lesions on NN plants, but was below the detection limit in systemic tissues of nn plants, which, in contrast, provided RNA readily when the TMVcp6xHis-2 plasmid was used as inoculum. Direct sequence analysis of the RT-PCR products confirmed that the 6xHis as well as the E50Q progeny had retained the engineered mutations and had not undergone revertant or second site CP mutations (data not shown).

wtTMV particles were successfully isolated from *N. tabacum* nn by use of method A, whereas 6xHis purification repeatedly failed, and E50Q revealed two bands after CsCl density-gradient centrifugation. The lower and fainter band complied with a buoyant density of 1.32, as for wtTMV (data not shown). The upper major band corresponded to a reduced density expected for RNA-free TMV protein assemblies. Electron microscopic analysis verified that both bands contained TMV-like particles of variable length (data not shown). In agreement with its lower buoyant density, no genomic TMV RNA was extractable from the predominant E50Q band, yielding further evidence that E50Q protein had assembled mainly into RNA-free particles.

3.2. Virus propagation and symptoms in different host plants

Since the initial purification of 6xHis from *N. tabacum* nn was insufficient, additional hosts were tested. Following mechanical inoculation with plasmid DNA, both mutants induced systemic symptoms (vein clearing and leaf curling) in *N. benthamiana* from 7 dpi on, which frequently developed to severe symptoms (14 dpi) and systemic necrosis at 28 dpi (Fig. 2). Symptoms varied and were even more enhanced in several combinations of the virus variants with different *N. rustica* types (Fig. 2). In the wild *N. rustica* variant, 6xHis or wtTMV provoked stunting and leaf necrosis, whereas E50Q primarily affected stems, resulting in death of adjoining leaves (Fig. 2). In the cultivar 'Cordata', pronounced stunting was observed with wtTMV and 6xHis, the latter of which also caused severe necrosis. By contrast, E50Q induced only few yellowing spots in systemically invaded leaves (Fig. 2). Finally, *N. rustica* 'Pavonii' showed similar symptoms for all virus variants, including stunting and expanded necrotic areas of systemic leaves (Fig. 2).

3.3. Virus isolation

N. benthamiana was used as an alternative host for isolation of the 6xHis mutant. Method A was applied for differential centrifugation, and combined with rate-zonal sucrose-gradient centrifugation. wtTMV was treated in parallel. As analyzed by Western blotting, part of the viral 6xHis particles accumulated in the same gradient fractions as wtTMV, but different from it, as the majority pelleted through the gradient, indicating a high tendency to aggregate for the mutant virus (data not shown). Upon SDS polyacrylamide gel electrophoresis, the 6xHis mutant exhibited considerable amounts of CP dimers and trimers retained in the gels, with apparent molecular weights of 36 and 54 kDa, respectively (data not shown).

Due to the differences in the behavior of the 6xHis particles compared to wtTMV during purification, method B was chosen as an alternative enrichment technique for all TMV variants. All intermediate fractions were scrutinized for the presence of viral particles by TEM, and the yields of the coat proteins from various plants and purification steps were quantified in two independent experiments using comparative and standardized Serva-violet 17 stained gels. Filtrates (F), pellets (P1), pellets (P2) and supernatants (S2) for wtTMV-, 6xHis- or E50Q-infected *N. benthamiana* plants were collected. In the filtrates, abundant CP was detected on Western blots for all TMV types (Fig. 3). wtTMV particles accumulated in the supernatant fractions S2 after butanol clarification (Fig. 3A), which was in contrast to both mutants that were mainly present in pellets (Fig. 3A; P1, P2) The majority of 6xHis protein (67/71% in two independent experiments, Table 3) was found in P1, whereas the majority of E50Q protein (54/63%, Table 3) was present in P2. Detection of the 6xHis CP extension with anti-His tag antisera confirmed the predominant presence of this protein in pellets P1 (Fig. 3B), and the maintenance of the CP modification.

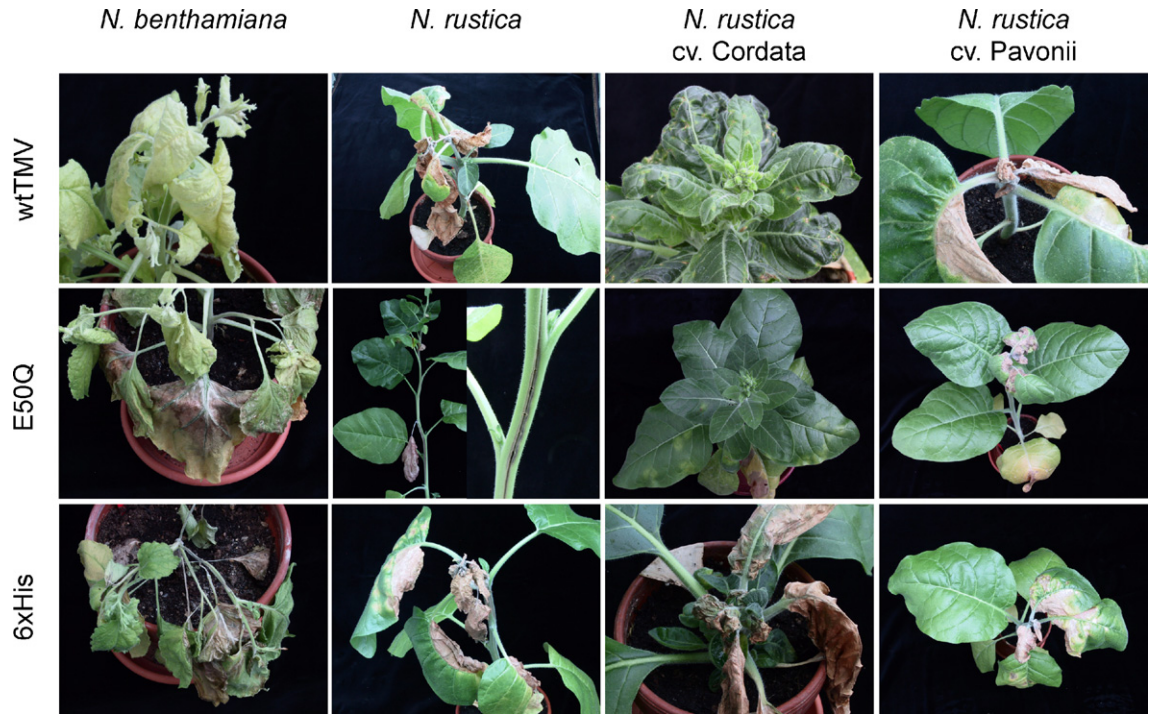

Fig. 2. Symptoms in different *Nicotiana* species or cultivars as indicated, after infection with the construct variants at 28 dpi. Note the high necrotic potential of 6xHis in different hosts, which may interfere with efficient virus purification. For details, refer to text.

Mass spectrometry (MALDI-MS) was used to analyze whether the His-tagged protein population was homogeneous. The analysis confirmed the unique presence of only one type of coat protein in each virion preparation, as obvious from single distinct mass peaks for every preparation (Fig. 3C). In order to further scrutinize the sequence identity of the viral progenies, plants were inoculated with the different variants (27 plants in total per virus in three independent experiments), total RNA was extracted from systemic leaves at 21 dpi, RT-PCR was applied to bacterially clone the CP cDNA, and 20–25 colonies were randomly selected for each variant and their insert DNA sequenced. The sequence analysis confirmed the sole presence of the intended mutants and ruled out any kind of reversion (data not shown).

3.4. Fate of RNA in the variants

In order to examine whether the mutant proteins were able to package the respective genomes, Northern blots were prepared representing all steps of the purification method B (Fig. 3D and E). wtTMV and the 6xHis viral RNAs co-purified with their proteins in all fractions, with most intense signals for wtTMV in S2 (Fig. 3D) and for 6xHis in P1 (Fig. 3D). In contrast, initial detection of RNA for E50Q failed for all fractions (Fig. 3D), although their CPs were abundantly present (Fig. 3A). Only after prolonged exposure (Fig. 3E), E50Q-RNA was detectable as faint bands in filtrate (F) and S2.

3.5. Variant particles after isopycnic density gradient centrifugation

Filtrate, pellet and supernatant fractions obtained from method B were processed in parallel for isopycnic Cs_2SO_4 centrifugation and the resulting fractions were analyzed by ELISA using anti-TMV antibodies (Fig. 4). The corresponding densities of the fractions were determined by refractometry, and ELISA values were drawn to the density scale. wtTMV particles with 5% RNA accumulated at densities of 1.29–1.33 g/cm^3 (Fig. 4; wtTMV; major peak), whereas RNA-free TMV protein was found in the upper fractions with densities of 1.25–1.27 g/cm^3 (Fig. 4; wtTMV; minor peaks). Most of wtTMV was retrieved from S2 as expected. Of the 6xHis particles from the first pellet fraction (P1), a small portion migrating at a density of 1.3 g/cm^3 indicated that at least some particles were formed with the canonical concentration of 5% RNA. However, the majority of their proteins were found in a broad distribution over the whole of the gradients, indicating that these particles are heterogeneous and have a tendency to decompose and/or aggregate with host components. E50Q protein, as expected from the previous experiments, was mainly found in RNA-free fractions with

Table 3
Relative accumulation (%) of TMV CP in fractions obtained by differential centrifugation.

	Purification steps according to method B[a]							
	F		P1		P2		S2	
Experiment	1	2	1	2	1	2	1	2
wtTMV	100	100	3.0	6.0	8.5	3.0	66.5	59.0
TMV-His_6	100	100	71.0	67.0	<0.3	<0.3	<0.3	<0.3
TMV-E50Q	100	100	2.0	0.5	62.5	53.5	<0.3	<0.3

[a] Values denote percentage amounts of TMV CP in systemically infected *N. benthamiana* leaves at 21 dpi in two independent experiments. TMV CP in the indicated fractions was quantified by means of dilution series analyzed via comparative SDS–PAGE after Serva-Violet staining. Absolute yields varied between experiments from 1.2 to 18 mg per g plant fresh weight with no significant differences between TMV variants.

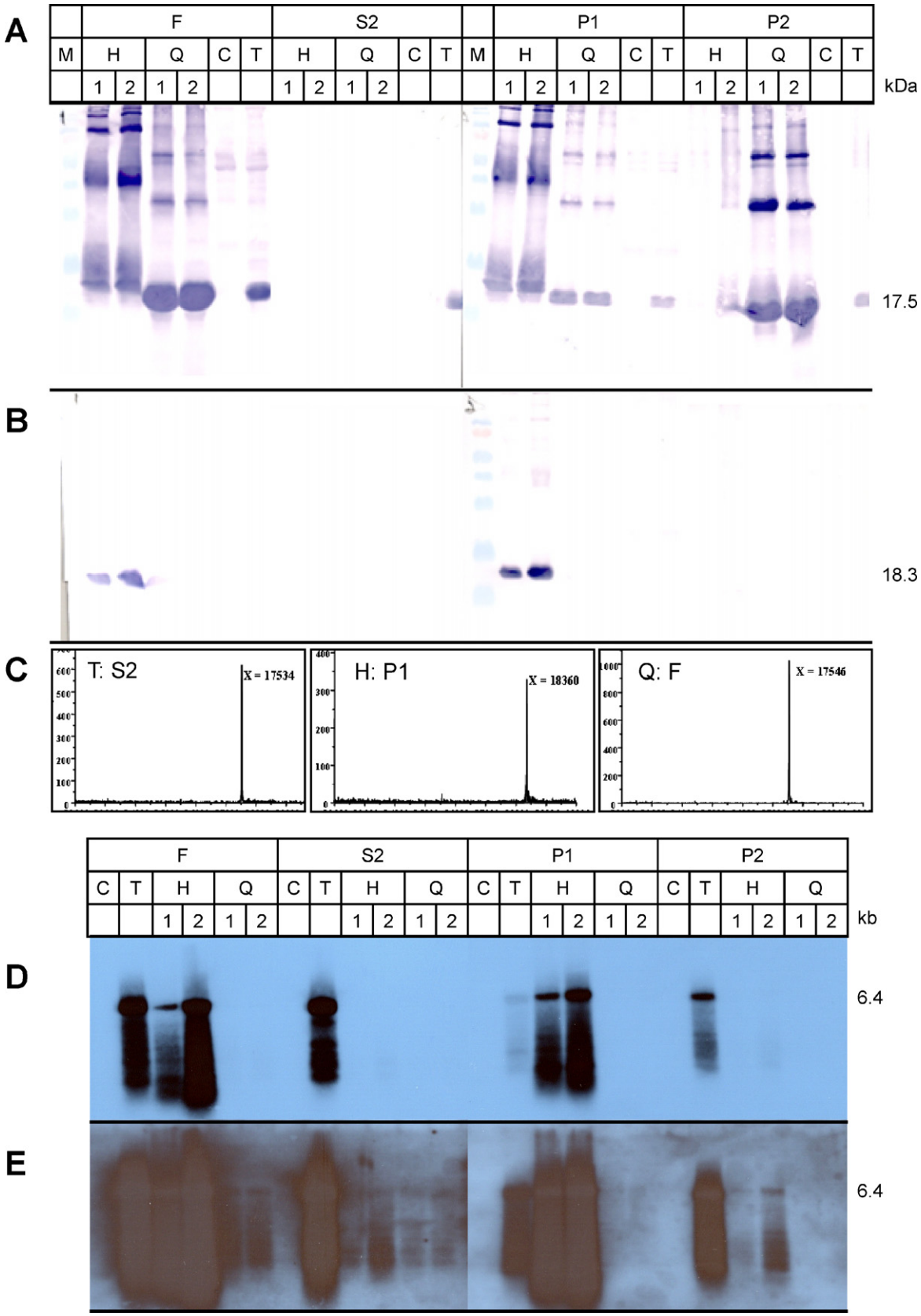

Fig. 3. Detection of CP and RNA for the four TMV variants during enrichment procedure (method B). Western blot (A, B), mass spectrometry analysis (C) and Northern blots (D and E) are shown for two independent *N. benthamiana* plant samples (lanes #1 and #2). Plants were inoculated with 6xHis (H), E50Q (Q) or wtTMV (T). Mock-inoculated *N. benthamiana* plants (C) served as negative control. Filtrates (F), supernatants (S2) and pellet fractions (P1) and (P2) are compared. Proteins were detected either with anti-TMV antibodies (A and B) or anti-pentaHis antibodies (B and D). M: prestained molecular weight marker (NEB). The calculated sizes of TMV CP (A) or His-tagged TMV CP (B) are indicated. MALDI-TOF spectra (C) of the respective proteins are indicated by the abbreviation of the variant and purification step from which they stem. Molecular masses are indicated above the single peak signals. RNA samples (D and E) were separated on SDS-agarose gels, blotted onto nylon membranes, and viral RNA was detected with a plus-strand-specific TMV CP RNA probe. (D) and (E) display the same blots with different exposure. The length of the TMV genome (6.4 kb) is indicated.

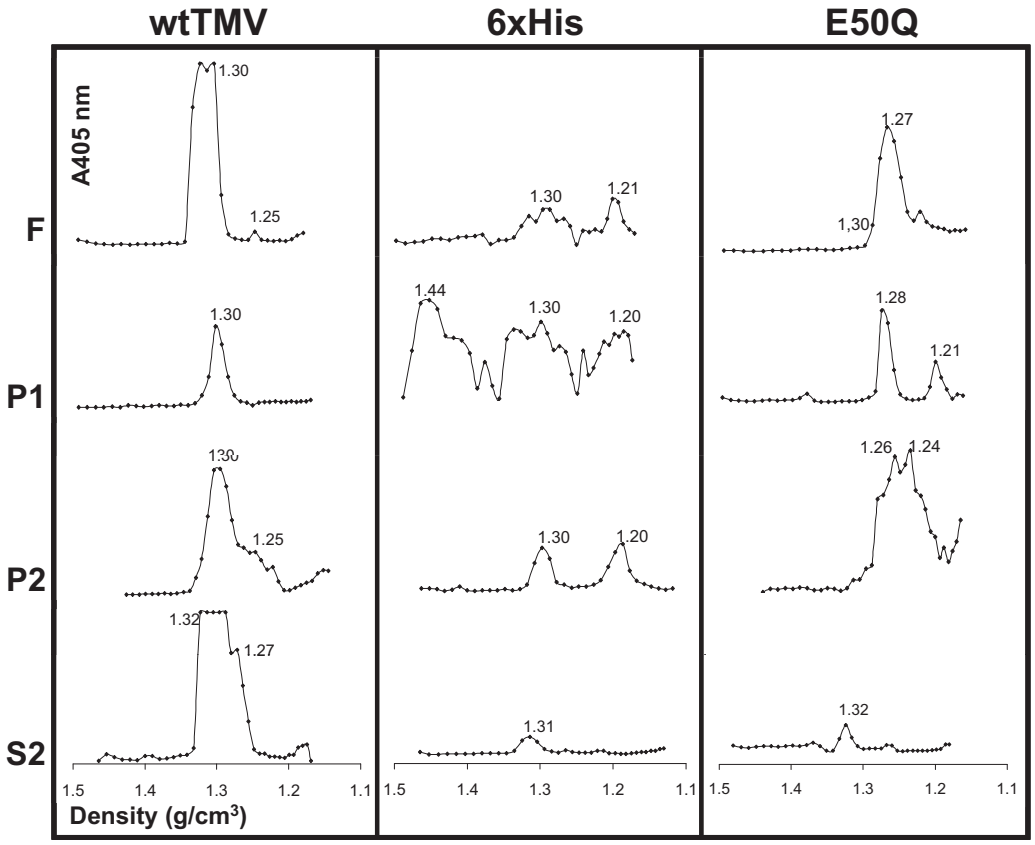

Fig. 4. Distribution of virions after different enrichment steps followed by isopycnic gradient centrifugation. *N. benthamiana* plant samples infected with the indicated TMV variants were processed by method B and filtrates (F), pellets (P1 and P2), and supernatants (S2) were collected. The respective fractions were separated in Cs_2SO_4 density gradients. Viral proteins were detected using anti-TMV antibodies in ELISA assays (absorption at 405 nm). Cesium densities of every second fraction were determined by refractive index measuring and interpolated for all fractions and used as × scale [g/cm^3]. The densities of prominent peak fractions are indicated [g/cm^3].

densities of 1.26–1.28 g/cm^3, with only a tiny peak for packaged RNA in S2 (Fig. 4).

3.6. Electron microscopy

The fractions obtained by method B were analyzed by negative staining and electron microscopy (Fig. 5). Rodlike 6xHis particles were present in the filtrate (data not shown) and in P1 (Fig. 5A), and tended to cluster considerably. E50Q particles were found in the filtrate (Fig. 5B) with extended length, frequently exceeding 2 μm. However, after butanol treatment, clumps of E50Q CPs accumulated and interfered with the detection of a low number of virus-like, but mostly short particles (P2 in Fig. 5C). wtTMV, as expected, revealed large amounts of typical helical rod-shaped particles about 300 nm in length in S2 (Fig. 5D). For E50Q, a few helical particles were found in P1 (not shown) and in S2 (Fig. 5E). Rare 6xHis virions with the shape of TMV were observed in P2 and S2 (Fig. 5F).

3.7. Differential metallization of variants

Filtrate-derived virus particles from wtTMV and both mutants (isolated via method B) were subjected to metallization reactions. After dialysis against water and subsequent electroless reductive nickel deposition (Knez et al., 2002), samples were analyzed by electron microscopy. Under the reaction conditions applied, nanowires up to 100 nm in length and with a diameter of 3 nm were formed within the central channel of the majority of E50Q particles, exceeding the number as well as the length of the wires produced in wtTMV in parallel (Fig. 6A–C). The length distributions of the nickel wires (Fig. 6E) showed a clear superiority of E50Q mutant- over wt TMV-templating.

The surface of the 6xHis particles directed a dense deposition of large nickel clusters to the outside of the virions (Fig. 6D). All particles resolved were covered completely with these metal clusters. A metallization of the outer surface has never been achieved with wtTMV in the absence of phosphate (Knez et al., 2004b) so far, hence the result is another clear indication for substantial changes in the viral 6xHis particles' surface chemistry.

4. Discussion

Distinct wild type or genetically modified full-length TMV cDNA constructs were suitable to infect various host plants by mechanical inoculation. In contrast to a previous report (Dagless et al., 1997), infection was efficiently achieved via mechanical inoculation of diverse *Nicotiana* species with viral cDNA, the transcription of which was driven by a 2x35S *Cauliflower mosaic virus* (CaMV) promoter. A maximum of 1 μg DNA per plant was sufficient to induce infection. As described for TMV in general (Zaitlin, 2000; Zaitlin and Israel, 1975) and for its mutants in particular (Culver, 2002; Mundry et al., 1990), the same inocula resulted in diverse plant responses, depending on the type and physiological state of the hosts. TMV CP amino acid alterations are known to contribute specifically to symptom determination, namely to the induction of chlorosis and necrosis (reviewed in Culver, 2002; Dawson, 1999). Necrotic Hypersensitive-Like Responses (HLR) occurring in otherwise systemic TMV hosts are a frequent obstacle upon the production of peptide-expressing or -coated TMV vectors, and recent evidence suggests mechanistic relations to HR such as mediated by the

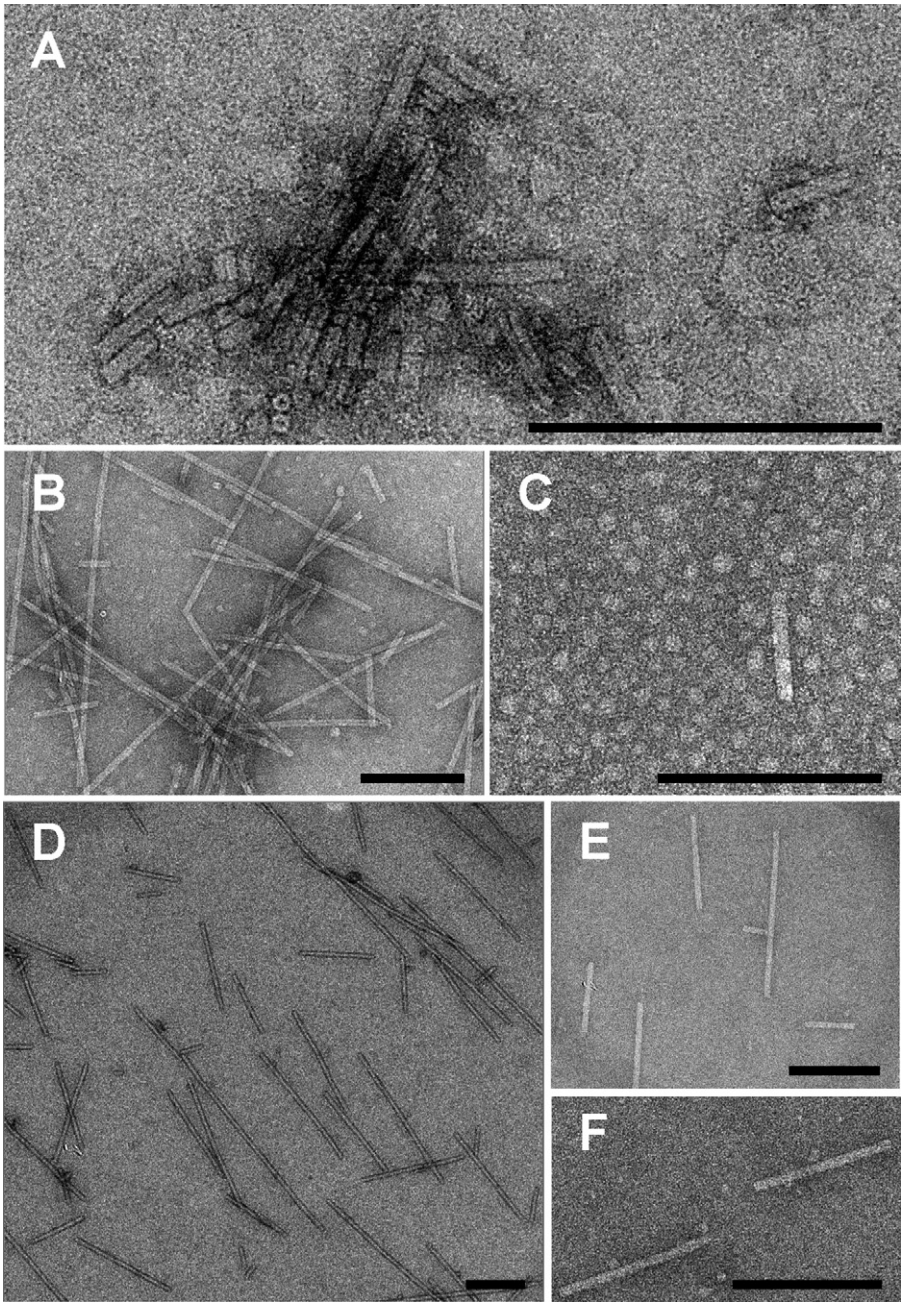

Fig. 5. Ultrastructure of TMV variants. ISEM micrographs of 6xHis (A and F), E50Q (B, C and E) and wtTMV (D) from method B steps P1 (A), F (B), P2 (C) and S2 (D, E and F). Specimens in negative contrast with uranyl acetate. Bars represent 300 nm.

N gene (Li et al., 2010b), but specific molecular signaling events have not been identified so far. It is often triggered by insertions at the carboxy terminus of the CP increasing its isoelectric point (Bendahmane et al., 1999). Consistent with these findings, both TMV variants 6xHis and E50Q elicited enhanced necrosis in some of the hosts (Fig. 2). For the production of TMV-based nanotemplates adapted to diverse current and forthcoming applications in biomedicine (Frolova et al., 2010; Li et al., 2010a; Smith et al., 2006), materials science (Soto and Ratna, 2010; Young et al., 2008), and technical sensing or catalytic devices (Gerasopoulos et al., 2010; Mao et al., 2009), it is therefore necessary to choose the hosts with the mildest symptoms, and to harvest the products early after infection. In the current study, *N. benthamiana* performed best amongst a number of plant types tested.

A C-terminal hexahistidine tail did not interfere with the structure of virions assembled *in planta* to a detectable extent, as has been reported for other short C-terminal insertions into TMV CP (Bendahmane et al., 1999). The E50Q mutation altering the Caspar-carboxylate composition stabilized the particles, whereby the capacity of systemic spread was reduced, as demonstrated previously (Culver et al., 1995; Lu et al., 1996); hence symptom development was delayed, and homogenates of systemic leaves did not induce HR in local lesion tests. E50Q proteins assembled mainly without the contribution of RNA but with extended length, consistent with former findings (Culver et al., 1995; Lu et al., 1996). Accordingly, the vast majority of the E50Q particles from systemically invaded tissues showed isopycnic densities (Fig. 4) characteristic of RNA-free assemblies (Zaitlin, 2000). How-

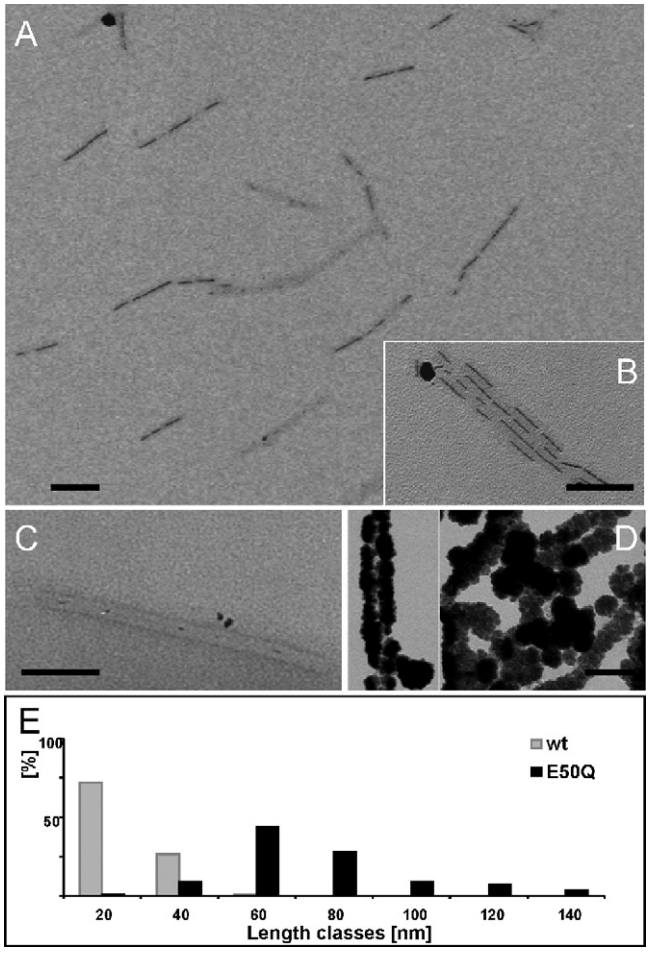

Fig. 6. TMV-based biotemplates after nickel metallization. Transmission electron microscopy in positive contrast for E50Q (A and B), wtTMV (C), and 6xHis (D). Method B filtrate fractions were adsorbed to grids after electroless deposition of nickel. Bars represent 100 nm. The length-distributions of nickel wires in the central channel for E50Q and wtTMV are compared (E). Histograms represent the percentage frequency distribution of nickel wires in the indicated length classes measured for wtTMV ($n = 114$) and E50Q ($n = 109$) wires.

ever, a small amount of E50Q particles that escaped degradation when treated with *n*-butanol, and thus was retained in the supernatant S2, was found to encapsidate RNA and to be approximately 300 nm in length. These particles presumably contained viral full-length RNA after systemic spread of the construct. The majority of E50Q particles had an increased length, which reflects the reduced repulsion between otherwise more negative electrostatic patches of adjacent CP subunits in this mutant lacking the carboxyl group of E50, which in wild type TMV is in close proximity to that of the D77 residue and contributes to the destabilization of the nucleoprotein helix in a suitable physicochemical environment (Culver et al., 1995; Kegel and van der Schoot, 2006; Namba and Stubbs, 1986). Nevertheless, butanol treatment was sufficient to disrupt the elongated protein assemblies lacking continuous RNA scaffolds (Fig. 5C).

Oligopeptides can be introduced on the outer face of TMV CPs without altering protein folding (Negrouk et al., 2004). Similarly, our hexahistidine fusion to the C-terminus did not prevent self-assembly and revealed particles which resembled wtTMV and packaged RNA. In isopycnic density gradient centrifugation (Fig. 4), a subfraction of the 6xHis particles exhibited the same buoyant density as wtTMV, but our data suggest that a significant portion disassembled under the high salt conditions. This may indicate that the hexahistidine tag reduced the virion stability. Moreover, the particles showed a high tendency to aggregate (Fig. 5A), which might be explained by an interaction of the His-tag with host nucleic acids and has been observed for further His-tagged protein species (Renzi et al., 2006). In addition, the 6xHis mutant induced necrotic reactions (Fig. 2) with the consequence of polyphenol accumulation and crosslinking of proteins. In this view, it is conceivable that large portions of dimers and multimers of 6xHis CP remained stable during SDS–PAGE (Fig. 3A). Interestingly, the TMV 6xHis CP, if expressed in yeast, did not assemble with RNA *in vitro* (Mueller et al., 2010).

In summary, despite of limitations upon the formation of homogeneous nucleoprotein nanotubes, both TMV CP mutants did not only allow accumulation of virion titers sufficient for subsequent applications in the inoculated leaves, they also were able to mediate long-distance (LD) transport of infectious nucleic acid via the vascular tissues – another essential function of the viral CP (Dawson et al., 1988). The CP's molecular roles upon systemic spread have not been unraveled, but several lines of evidence indicate that TMV virion formation is not required at this stage (Wisniewski et al., 1988, and references therein): tobamoviral CP mutations abolishing its assembly into helical particles did not prevent LD movement of the viral agent (e.g. Berzal-Herranz et al., 1995; Dawson et al., 1988); and, furthermore, LD trafficking of TMV lacking CP was complemented by a nonstructural protein of an umbravirus (Ryabov et al., 1999). Putative roles of TMV CP upon systemic spread may therefore encompass gating the transported complex into companion cell/sieve element domains inside the phloem, maybe as accessory function supporting the viral movement protein (Heinlein, 2002; Ryabov et al., 1999, and references therein), and/or interactions with host factors directly or indirectly enabling long-distance transport in vascular tissues (Li et al., 2005).

As with our previous studies (Balci et al., 2006; Knez et al., 2002, 2003, 2004b), the new TMV variants were successfully metallized with nickel. The electroless deposition process requires to firstly bind Pd(II) in an "activation" step. In the absence of phosphate, a reaction with carboxylate groups is possible; they dominate the surface chemistry especially in the channel of wtTMV and E50Q particles. However, nitrogen ligands and namely His are favored, so a faster reaction and dense exterior coating of the 6xHis nanotubes was expected. Catalytically active Pd nanoparticles ($d < 4$ nm) are then formed by reduction of Pd(II) to Pd(0), and by coalescence. Since the metallization by nickel is autocatalytic, Ni initially deposited on Pd as well as subsequently on Pd/Ni nuclei. catalyzes its own deposition, with the required electrons produced by catalytic oxidation of BH_3 (from $(CH_3)_2NH{\cdot}BH_3$).

Therefore, the 6xHis mutant was metallized specifically on its outer coat without any further treatment, where Pd(II) was bound to the His-tags. On the outer surface of wtTMV, nickel accumulation can be induced by phosphate conditioning (Knez et al., 2004b). In contrast, for wtTMV and the E50Q virions, Pd is predominantly directed into the channel promoting Ni nanowire growth (Knez et al., 2002). Interestingly, the wires inside the E50Q mutant particles were significantly longer and formed with increased efficiency in comparison to those inside wtTMV virions under the conditions applied (Fig. 6E). The channel chemistry should be identical for both virus variants, as the E50Q mutation affects inaccessible parts of the virions. However, probably due to their enhanced stability against chemical and physical changes, the in many cases very long (up to some micrometers) virus-like tubes seem to allow for a largely unhindered growth of metal wires of improved quality. Assumedly also the absence of the RNA scaffold renders beneficial conditions for reductive nickel deposition.

In conclusion, this study demonstrates that genetic engineering of the tubular plant virus has resulted in new types of biotemplates that governed the final nanostructure of inorganic reaction products in a predictable manner. Inner-surface metallization of the

stiff helical capsids may offer a unique access to ultrathin interconnects for nanoscale circuits (Kwok and Ellenbogen, 2002), or to printable nanoelectronic arrays (Fan et al., 2009). Magnetic metal coatings of TMV-derived particles with pre-determined aspect ratio might contribute to a novel production route for high-performance nanotube ferrofluids applied for damping purposes in micromechanical devices: support for this concept comes from our recent results demonstrating the stable and tunable beneficial effects of tobamoviral scaffolding additives on commercially available nanosphere ferrofluids (Wu et al., 2010a,b).

Acknowledgements

The authors thank the gardeners for taking care of the plants, Sigrid Kober and Sylvia Pfeiffer for excellent technical assistance, and Katharina Kittelmann, Robert G. Milne and Carl Krill for critically reading the manuscript. This work was funded by the Baden-Wuerttemberg-Stiftung, "Kompetenznetz Funktionelle Nanostrukturen", and subsidiarily supported by the DFG-SPP1165.

References

Balci, S., Bittner, A., Schirra, M., Thonke, K., Sauer, R., Hahn, K., Kadri, A., Wege, C., Jeske, H., Kern, K., 2009. Catalytic coating of virus particles with zinc oxide. Electrochim. Acta 54, 5149–5154.

Balci, S., Bittner, A.M., Hahn, K., Scheu, C., Knez, M., Kadri, A., Wege, C., Jeske, H., Kern, K., 2006. Copper nanowires within the central channel of tobacco mosaic virus particles. Electrochim. Acta 51, 6251–6257.

Balci, S., Leinberger, D.M., Knez, M., Bittner, A.M., Boes, F., Kadri, A., Wege, C., Jeske, H., Kern, K., 2008. Printing and aligning mesoscale patterns of tobacco mosaic viruses on surfaces. Adv. Mater. 20, 2195–2200.

Balci, S., Noda, K., Bittner, A.M., Kadri, A., Wege, C., Jeske, H., Kern, K., 2007. Self-assembly of metal-virus nanodumbbells. Angew. Chem. Int. Ed. 46, 3149–3151.

Bendahmane, M., Chen, I., Asurmendi, S., Bazzini, A.A., Szecsi, J., Beachy, R.N., 2007. Coat protein-mediated resistance to TMV infection of *Nicotiana tabacum* involves multiple modes of interference by coat protein. Virology 366, 107–116.

Bendahmane, M., Koo, M., Karrer, E., Beachy, R.N., 1999. Display of epitopes on the surface of tobacco mosaic virus: impact of charge and isoelectric point of the epitope on virus–host interactions. J. Mol. Biol. 290, 9–20.

Berzal-Herranz, A., de la Cruz, A., Tenllado, F., Diaz-Ruiz, J.R., Lopez, L., Sanz, A.I., Vaquero, C., Serra, M.T., Garcia-Luque, I., 1995. The Capsicum L3 gene-mediated resistance against the tobamoviruses is elicited by the coat protein. Virology 209, 498–505.

Boom, R., Sol, C.J.A., Salimans, M.M.M., Jansen, C.L., Wertheim-van Dillen, P.M.E., van der Noordaa, J., 1990. Rapid and simple method for purification of nucleic acids. J. Clin. Microbiol. 28, 495–503.

Caspar, D.L.D., 1963. Assembly and stability of the tobacco mosaic virus particle. Adv. Protein Chem. 18, 37–121.

Caspar, D.L.D., Namba, K., 1990. Switching in the self-assembly of tobacco mosaic virus. Adv. Biophys. 26, 157–185.

Chapman, S.N., 1998. Tobamovirus isolation and RNA extraction. In: Foster, G.D., Taylor, S.C. (Eds.), Methods in Molecular Biology: Plant Virology Protocols: From Virus Isolation to Transgenic Resistance, vol. 81. Humana Press Inc., Totowa, NJ, pp. 123–129.

Clare, D.K., Orlova, E.V., 2010. 4.6 Å Cryo-EM reconstruction of tobacco mosaic virus from images recorded at 300 keV on a 4k × 4k CCD camera. J. Struct. Biol., 303–308.

Culver, J.N., 2002. Tobacco mosaic virus assembly and disassembly: determinants in pathogenicity and resistance. Annu. Rev. Phytopathol. 40, 287–308.

Culver, J.N., Dawson, W.O., Plonk, K., Stubbs, G., 1995. Site-directed mutagenesis confirms the involvement of carboxylate groups in the disassembly of tobacco mosaic virus. Virology 206, 724–730.

Dagless, E.M., Shintaku, M.H., Nelson, R.S., Foster, G.D., 1997. A CaMV 35S promoter driven cDNA clone of tobacco mosaic virus can infect host plant tissue despite being uninfectious when manually inoculated onto leaves. Arch. Virol. 142, 183–191.

Dawson, W.O., 1999. Tobacco mosaic virus virulence and avirulence. Philos. Trans. R. Soc. Lond. B: Biol. Sci. 354, 645–651.

Dawson, W.O., Bubrick, P., Grantham, G.L., 1988. Modifications of the tobacco mosaic virus coat protein gene affecting replication, movement, and symptomatology. Phytopathology 78, 783–789.

Devash, Y., Hauschner, A., Sela, I., Chakraburtty, K., 1981. The Anti-Viral Factor (Avf) from virus-infected plants induces discharge of Histidinyl-Tmv-Rna. Virology 111, 103–112.

Dujardin, E., Peet, C., Stubbs, G., Culver, J.N., Mann, S., 2003. Organization of metallic nanoparticles using tobacco mosaic virus templates. Nano Lett. 3, 413–417.

Fan, Z., Ho, J.C., Takahashi, T., Yerushalmi, R., Takei, K., Ford, A.C., Chueh, Y.-L., Javey, A., 2009. Toward the development of printable nanowire electronics and sensors. Adv. Mater. 21, 3730–3743.

Frolova, O.Y., Petrunia, I.V., Komarova, T.V., Kosorukov, V.S., Sheval, E.V., Gleba, Y.Y., Dorokhov, Y.L., 2010. Trastuzumab-binding peptide display by tobacco mosaic virus. Virology 407, 7–13.

Gerasopoulos, K., McCarthy, M., Banerjee, P., Fan, X., Culver, J.N., Ghodssi, R., 2010. Biofabrication methods for the patterned assembly and synthesis of viral nanotemplates. Nanotechnology 21, 11, 055304.

Górzny, M., Walton, A.S., Evans, S.D., 2010. Synthesis of high-surface-area platinum nanotubes using a viral template. Adv. Funct. Mater. 20, 1295–1300.

Heinlein, M., 2002. The spread of tobacco mosaic virus infection: insights into the cellular mechanism of RNA transport. Cell. Mol. Life Sci. 59, 58–82.

Kegel, W.K., van der Schoot, P., 2006. Physical regulation of the self-assembly of tobacco mosaic virus coat protein. Biophys. J. 91, 1501–1512.

Klug, A., 1999. The tobacco mosaic virus particle: structure and assembly. Philos. Trans. R. Soc. Lond. B 354, 531–535.

Knez, M., Bittner, A.M., Boes, F., Wege, C., Jeske, H., Maiß, E., Kern, K., 2003. Biotemplate synthesis of 3-nm nickel and cobalt nanowires. Nano Lett. 3, 1079–1082.

Knez, M., Kadri, A., Wege, C., Gosele, U., Jeske, H., Nielsch, K., 2006. Atomic layer deposition on biological macromolecules: metal oxide coating of tobacco mosaic virus and ferritin. Nano Lett. 6, 1172–1177.

Knez, M., Sumser, M., Bittner, A., Wege, C., Jeske, H., Hoffmann, D.M.P., Kuhnke, K., Kern, K., 2004a. Binding the tobacco mosaic virus to inorganic surfaces. Langmuir 20, 411–447.

Knez, M., Sumser, M., Bittner, A.M., Wege, C., Jeske, H., Kooi, S., Burghard, M., Kern, K., 2002. Electrochemical modification of individual nano-objects. J. Electroanal. Chem. 522, 70–74.

Knez, M., Sumser, M., Bittner, A.M., Wege, C., Jeske, H., Martin, T.P., Kern, K., 2004b. Spatially selective nucleation of metal clusters on the tobacco mosaic virus. Adv. Funct. Mater. 14, 116–124.

Kobayashi, M., Seki, M., Tabata, H., Watanabe, Y., Yamashita, I., 2010. Fabrication of aligned magnetic nanoparticles using tobamoviruses. Nano Lett. 10, 773–776.

Kwok, K.S., Ellenbogen, J.C., 2002. Moletronics: future electronics. Mater. Today 5, 28–37.

Laemmli, U.K., 1970. Cleavage of structural proteins during the assembly of the head of bacteriophage T4. Nature 227, 680–685.

Lee, S.Y., Choi, J., Royston, E., Janes, D.B., Culver, J.N., Harris, M.T., 2006. Deposition of platinum clusters on surface-modified tobacco mosaic virus. J. Nanosci. Nanotechnol. 6, 974–981.

Lee, S.Y., Royston, E., Culver, J.N., Harris, M.T., 2005. Improved metal cluster deposition on a genetically engineered tobacco mosaic virus template. Nanotechnology 16, S435–S441.

Li, K., Nguyen, H.G., Lu, X., Wang, Q., 2010a. Viruses and their potential in bioimaging and biosensing applications. Analyst 135, 21–27.

Li, M., Li, P., Song, R., Xu, Z., 2010b. An induced hypersensitive-like response limits expression of foreign peptides via a recombinant TMV-based vector in a susceptible tobacco. PLoS ONE 5, e15087.

Li, Y., Wu, M.Y., Song, H.H., Hu, X., Qiu, B.S., 2005. Identification of a tobacco protein interacting with tomato mosaic virus coat protein and facilitating long-distance movement of virus. Arch. Virol. 150, 1993–2008.

Lim, J.S., Kim, S.M., Lee, S.Y., Stach, E.A., Culver, J.N., Harris, M.T., 2010. Formation of Au/Pd alloy nanoparticles on TMV. J. Nanomater. 2010, 6, 620505.

Lu, B., Stubbs, G., Culver, J.N., 1996. Carboxylate interactions involved in the disassembly of tobacco mosaic tobamovirus. Virology 225, 11–20.

Mao, C., Liu, A., Cao, B., 2009. Virus-based chemical and biological sensing. Angew. Chem. Int. Ed. 48, 6790–6810.

Miller, R.A., Presley, A.D., Francis, M.B., 2007. Self-assembling light-harvesting systems from synthetically modified tobacco mosaic virus coat proteins. J. Am. Chem. Soc. 129, 3104–3109.

Milne, R.G., Lesemann, D.E., 1984. Immunosorbent electron microscopy in plant virus studies. In: Maramorosch, K., Koprowski, H. (Eds.), Methods in Virology, vol. VIII. Academic Press, San Diego, pp. 85–101.

Mueller, A., Kadri, A., Jeske, H., Wege, C., 2010. In vitro assembly of tobacco mosaic virus coat protein variants derived from fission yeast expression clones or plants. J. Virol. Methods 166, 77–85.

Mundry, K.W., Schaible, W., Ellwart-Tschürtz, M., Nitschko, H., Hapke, C., 1990. Hypersensitivity to tobacco mosaic virus in N′-gene hosts: which viral genes are involved? In: Fraser, R.S.S. (Ed.), Recognition and Response in Plant–Virus Interactions, vol. H41. Springer-Verlag, Berlin/Heidelberg, pp. 345–359.

Mutombo, K., Michels, B., Ott, H., Cerf, R., Witz, J., 1992. Scanning calorimetric studies of the stability of tobacco mosaic virus and aggregates of its coat protein. Eur. Biophys. J. 21, 77–83.

Namba, K., Pattanayek, R., Stubbs, G., 1989. Visualization of protein-nucleic acid interactions in a virus. Refined structure of intact tobacco mosaic virus at 2.9 Å resolution by X-ray fiber diffraction. J. Mol. Biol. 208, 307–325.

Namba, K., Stubbs, G., 1986. Structure of tobacco mosaic virus at 3.6 Å resolution: implications in assembly. Science 231, 1401–1406.

Negrouk, V., Eisner, G., Midha, S., Lee, H., Bascomb, N., Gleba, Y., 2004. Affinity purification of streptavidin using tobacco mosaic virus particles as purification tags. Anal. Biochem. 333, 230–235.

Perham, R.N., Wilson, T.M.A., 1978. The characterization of intermediates formed during disassembly of tobacco mosaic virus at alkaline pH. Virology 84, 293–302.

Renzi, F., Panetta, G., Vallone, B., Brunori, M., Arceci, M., Bozzoni, I., Laneve, P., Caffarelli, E., 2006. Large-scale purification and crystallization of the endoribonuclease XendoU: troubleshooting with His-tagged proteins. Acta Crystall. F: Struct. Biol. Cryst. Commun. 62, 298–301.

Restrepo, M.A., Freed, D.D., Carrington, J.C., 1990. Nuclear transport of plant potyviral proteins. Plant Cell 2, 987–998.

Rong, J.H., Oberbeck, F., Wang, X.N., Li, X.D., Oxsher, J., Niu, Z.W., Wang, Q., 2009. Tobacco mosaic virus templated synthesis of one dimensional inorganic-polymer hybrid fibres. J. Mater. Chem. 19, 2841–2845.
Royston, E., Ghosh, A., Kofinas, P., Harris, M.T., Culver, J.N., 2008. Self-assembly of virus-structured high surface area nanomaterials and their application as battery electrodes. Langmuir 24, 906–912.
Royston, E.S., Brown, A.D., Harris, M.T., Culver, J.N., 2009. Preparation of silica stabilized tobacco mosaic virus templates for the production of metal and layered nanoparticles. J. Colloid Interface Sci. 332, 402–407.
Ryabov, E.V., Robinson, D.J., Taliansky, M.E., 1999. A plant virus-encoded protein facilitates long-distance movement of heterologous viral RNA. Proc. Natl. Acad. Sci. U.S.A. 96, 1212–1217.
Sachse, C., Chen, J.Z., Coureux, P.D., Stroupe, M.E., Fandrich, M., Grigorieff, N., 2007. High-resolution electron microscopy of helical specimens: a fresh look at tobacco mosaic virus. J. Mol. Biol. 371, 812–835.
Sambrook, J., Russell, D.W., 2001. Molecular Cloning: A Laboratory Manual, 3rd ed. Cold Spring Harbor Laboratory Press, Cold Spring Harbor, NY.
Schlick, T.L., Ding, Z., Kovacs, E.W., Francis, M.B., 2005. Dual-surface modification of the tobacco mosaic virus. J. Am. Chem. Soc. 127, 3718–3723.
Shenton, W., Douglas, T., Young, M., Stubbs, G., Mann, S., 1999. Inorganic–organic nanotube composites from template mineralization of tobacco mosaic virus. Adv. Mater. 11, 253–256.
Shintaku, M.H., Carter, S.A., Bao, Y., Nelson, R.S., 1996. Mapping nucleotides in the 126-kDa protein gene that control the differential symptoms induced by two strains of tobacco mosaic virus. Virology 221, 218–225.
Smith, M.L., Lindbo, J.A., Dillard-Telm, S., Brosio, P.M., Lasnik, A.B., McCormick, A.A., Nguyen, L.V., Palmer, K.E., 2006. Modified tobacco mosaic virus particles as scaffolds for display of protein antigens for vaccine applications. Virology 348, 475–488.
Soto, C.M., Ratna, B.R., 2010. Virus hybrids as nanomaterials for biotechnology. Curr. Opin. Biotechnol. 21, 426–438.
Towbin, H., Staehelin, T., Gordon, J., 1979. Electrophoretic transfer of proteins from polyacrylamide gels to nitrocellulose sheets: procedure and some applications. Proc. Natl. Acad. Sci. U.S.A. 76, 4350–4354.
Tseng, R.J., Tsai, C., Ma, L.P., Ouyang, J., Ozkan, C.S., Yang, Y., 2006. Digital memory device based on tobacco mosaic virus conjugated with nanoparticles. Nat. Nanotechnol. 1, 72–77.
Wisniewski, L.A., Powell, P.A., Nelson, R.S., Beachy, R.N., 1988. Local and systemic spread of tobacco mosaic virus in transgenic tobacco. Plant Cell 2, 559–567.
Wu, Z., Mueller, A., Degenhard, S., Ruff, S.E., Geiger, F., Bittner, A., Wege, C., Krill III, C., 2010a. Enhancing the magnetoviscosity of ferrofluids by the addition of biological nanotubes. ACS Nano 4, 4531–4538.
Wu, Z., Zierold, R., Mueller, A., Ruff, S.E., Ma, C., Khan, A.A., Geiger, F., Sommer, B.A., Knez, M., Nielsch, K., Bittner, A.M., Wege, C., Krill III, C., 2010b. Preparation and magnetoviscosity of nanotube ferrofluids by viral scaffolding and ALD on porous templates. Phys. Stat. Sol. B, 2412–2423.
Yang, C., Manocchi, A.K., Lee, B., Yi, H., 2010. Viral templated palladium nanocatalysts for dichromate reduction. Appl. Catal. B: Environ. 93, 282–291.
Yi, H., Nisar, S., Lee, S.Y., Powers, M.A., Bentley, W.E., Payne, G.F., Ghodssi, R., Rubloff, G.W., Harris, M.T., Culver, J.N., 2005. Patterned assembly of genetically modified viral nanotemplates via nucleic acid hybridization. Nano Lett. 5, 1931–1936.
Young, M., Willits, D., Uchida, M., Douglas, T., 2008. Plant viruses as biotemplates for materials and their use in nanotechnology. Annu. Rev. Phytopathol. 46, 361–384.
Zaitlin, M., 2000. Tobacco mosaic virus. AAB Descr. Plant Viruses 370, 1–13.
Zaitlin, M., Israel, H.W., 1975. Tobacco mosaic virus (type strain). C.M.I./A.A.B. Descr. of Plant Viruses, No. 151.